Effect of Element Directivity on Adaptive Beamforming Applied to High-Frame-Rate Ultrasound

Hideyuki Hasegawa and Hiroshi Kanai

Abstract—High-frame-rate ultrasound is a promising technique for measurement and imaging of cardiovascular dynamics. In high-frame-rate ultrasonic imaging, unfocused ultrasonic beams are used in transmit and multiple focused receiving beams are created by parallel beamforming using the delay and sum (DAS) method. However, the spatial resolution and contrast are degraded compared with conventional beamforming using focused transmit beams. In the present study, the minimum variance beamformer was examined for improvement of the spatial resolution in high-frame-rate ultrasound. In conventional minimum variance beamforming, the spatial covariance matrix of ultrasonic echo signals received by individual transducer elements is obtained without considering the directivity of the transducer element. By omitting the element directivity, the error in estimation of the desired signal (i.e., the echo from the focal point) increases, and as a result, the improvement of the spatial resolution is degraded. In the present study, the element directivity was taken into account in estimation of the spatial covariance matrix used in minimum variance beamforming. The effect of the element directivity on adaptive beamforming was evaluated by computer simulation and basic experiments using a phantom. In parallel beamforming with the conventional DAS beamformer, the lateral spatial resolution, which was evaluated from the lateral full width at half maximum of the echo amplitude profile in the basic experiment, was 0.50 mm. Using conventional amplitude and phase estimation (APES) beamforming, the lateral spatial resolution was improved to 0.37 mm. The lateral spatial resolution was further improved to 0.30 mm using the modified APES beamforming by considering the element directivity. Image contrast and contrast-to-noise ratios, respectively, were −12.3 and 6.5 dB (DAS), −32.8 and −11.3 dB (APES), and −7.0 and 3.1 dB (modified APES).

I. Introduction

MEASUREMENTS of cardiovascular dynamics and viscoelasticity are useful for diagnosis of the cardiovascular system. High-frame-rate ultrasound is a promising technique for measurement and imaging of tissue dynamics. High-frame-rate ultrasound using parallel beamforming, which was introduced in the 1980s [1], basically uses unfocused transmit beams and creates multiple focused receiving beams in each transmission. The first practical application of high-frame-rate ultrasound was the measurement of the displacement distribution in biological tissue induced by acoustic radiation force [2]. This technique is very useful for assessment of tissue viscoelasticity noninvasively. Recently, we have shown that high-frame-rate ultrasound is also useful for B-mode, tissue strain, and blood flow imaging [3]. Currently, various methods based on high-frame-rate imaging have been developed for measurement of cardiovascular dynamics [4]–[10].

One of the problems of high-frame-rate imaging is the degradation of spatial resolution owing to the use of unfocused transmit beams and, thus, development of methods for improvement of spatial resolution is desired to simultaneously realize high temporal and spatial resolutions. The spatial compound technique [11] is one method for improvement of the spatial resolution in high-frame-rate imaging [12]. In the cited study, the image spatial resolution was shown to be significantly improved by coherently compounding multiple steered plane waves. However, multiple transmissions of plane waves degrades the imaging frame rate.

Recently, adaptive beamforming, namely, minimum variance beamforming, has been introduced to ultrasound imaging for improvement of the spatial resolution [13]–[16]. In the beamforming procedure, ultrasonic echo signals received by individual transducer elements in an ultrasonic probe are aligned based on the geometrical information of the focal point and then averaged. This way of beamforming is called the delay and sum (DAS) method. The weights given to the element echo signals in the averaging procedure are fixed, and a tapered weighting function, such as the Hann function, is typically used. In adaptive beamforming, those weights are adaptively determined using the received ultrasonic echoes, and this procedure improves the spatial resolution significantly. Recently, minimum variance beamforming was combined with synthetic transmit beamforming for high-frame-rate echocardiography [17].

In minimum variance beamforming, the spatial covariance matrix of the received element echo signals is estimated to determine the weights to the element echo signals. In this procedure, the desired signal (echo from the focal point) is suppressed when the desired signal is contained in the spatial covariance matrix. Sub-array averaging was introduced to remove the desired signal from the spatial covariance matrix. Using sub-array averaging,

suppression of the desired signal is avoided at the expense of the spatial resolution [14]. Sub-array averaging is also contribute to reduce the dimension of the spatial covariance matrix. Furthermore, temporal or depth averaging is required to obtain speckle statistics similar to that obtained by conventional DAS beamforming [18]. Reduction of computational load, such as reduction of the dimension of the spatial covariance matrix, is very important for real-time implementation and is studied intensively [19]–[21].

Alternative way to remove the desired signal from the spatial covariance matrix is to estimate the desired signal from the received element signals. Blomberg *et al.* proposed the amplitude and phase estimation (APES) beamforming, in which the desired signal is estimated by DAS beamforming [22]. However, in their study, the directivity of the transducer element is not considered in estimation of the desired signal. In the present study, the element directivity was incorporated to improve the accuracy in estimation of the desired signal. Such improvement would reduce the suppression of the desired signal in the APES beamforming.

II. MATERIALS AND METHODS

A. Conventional Delay and Sum (DAS) Beamforming

Let us define the complex signal of the ultrasonic echo received by the mth transducer element of an ultrasonic probe by s_m ($m = 0, 1, 2, ..., M-1$), where M is the total number of elements in the aperture. The M signals are ordered in a vector as follows:

$$\mathbf{S} = (s_0 \ s_1 \ ... \ s_{M-1})^{\mathrm{T}}, \tag{1}$$

where T denotes the transpose. The lateral position of the mth transducer element is defined by x_m and the range position z of every transducer element is zero. By defining the position of the receiving focal point to be $(x_{\mathrm{f}}, z_{\mathrm{f}})$, the output u_{DS} of the DAS beamformer is expressed as follows:

$$u_{\mathrm{DS}} = \mathbf{w}_{\mathrm{DS}}^{\mathrm{H}}\mathbf{S}, \tag{2}$$

where H is the Hermitian operator. In (2), w_{DS} shows the weights for the element signals used in DAS beamforming. In the present study, for an easy comparison between the physical meanings of the adaptive and conventional DAS beamformers, rectangular apodization is considered in conventional DAS beamforming. In the case of rectangular apodization, (2) is expressed as follows:

$$\mathbf{w}_{\mathrm{DS}} = \frac{\mathbf{a}}{\mathbf{a}^{\mathrm{H}}\mathbf{a}} = \frac{\mathbf{I}^{-1}\mathbf{a}}{\mathbf{a}^{\mathrm{H}}\mathbf{I}^{-1}\mathbf{a}}, \tag{3}$$

where $\mathbf{I}$ is the identity matrix, and $\mathbf{a}$ is called the steering vector, expressed as

$$\mathbf{a} = \begin{pmatrix} a_0 \\ a_1 \\ \vdots \\ a_{M-1} \end{pmatrix} = \begin{pmatrix} \exp\left(-j\dfrac{2\pi f_0\sqrt{(x_0 - x_f)^2 + z_f^2}}{c_0}\right) \\ \exp\left(-j\dfrac{2\pi f_0\sqrt{(x_1 - x_f)^2 + z_f^2}}{c_0}\right) \\ \vdots \\ \exp\left(-j\dfrac{2\pi f_0\sqrt{(x_{M-1} - x_f)^2 + z_f^2}}{c_0}\right) \end{pmatrix}, \tag{4}$$

where f_0 is the ultrasonic center frequency, and c_0 is the speed of sound.

B. Adaptive Beamforming

As in conventional DAS beamforming, the output u_{MV} of the adaptive beamformer, namely, minimum variance beamformer, is expressed as follows:

$$u_{\mathrm{MV}} = \mathbf{w}_{\mathrm{MV}}^{\mathrm{H}}\mathbf{S}. \tag{5}$$

The minimum variance beamformer determines the weight $\mathbf{w}_{\mathrm{MV}}$ so as to minimize the variance P of the output u_{MV} [13], [14]. The variance (power) P of the output u_{MV} is expressed as follows:

$$P = \mathrm{E}[|u_{\mathrm{MV}}|^2] = \mathrm{E}[\mathbf{w}_{\mathrm{MV}}^{\mathrm{H}}\mathbf{S}\mathbf{S}^{\mathrm{H}}\mathbf{w}_{\mathrm{MV}}] = \mathbf{w}_{\mathrm{MV}}^{\mathrm{H}}\mathbf{R}\mathbf{w}_{\mathrm{MV}}, \tag{6}$$

where $\mathrm{E}[\cdot]$ denotes the expectation, and $\mathbf{R}$ is the spatial covariance matrix and expressed as follows:

$$\mathbf{R} = \mathrm{E}[\mathbf{S}\mathbf{S}^{\mathrm{H}}]. \tag{7}$$

This minimization problem can be expressed as follows:

$$\min_{\mathbf{w}_{\mathrm{MV}}} \mathbf{w}_{\mathrm{MV}}^{\mathrm{H}}\mathbf{R}\mathbf{w}_{\mathrm{MV}}, \text{ subject to } \mathbf{w}_{\mathrm{MV}}^{\mathrm{H}}\mathbf{a} = 1. \tag{8}$$

The solution to (8) is expressed as follows:

$$\mathbf{w}_{\mathrm{MV}} = \frac{\mathbf{R}^{-1}\mathbf{a}}{\mathbf{a}^{\mathrm{H}}\mathbf{R}^{-1}\mathbf{a}}. \tag{9}$$

As can be seen in (9), the weight $\mathbf{w}_{\mathrm{MV}}$ determined by the minimum variance beamformer has a form very similar to that of the DAS beamformer expressed by (3). In (3), the identity matrix is used as the covariance matrix. This means that undesired signals, which are suppressed by the DAS beamformer, are uncorrelated with each other (i.e., the covariance matrix of such components becomes the identity matrix). On the other hand, in minimum variance beamforming, the spatial covariance matrix, which corresponds to the undesired signals to be suppressed, is determined from the measured signal $\mathbf{S}$. However, the measured signal $\mathbf{S}$ contains the desired signal (i.e., the echo from the focal point). Therefore, the desired signal would also be suppressed when the spatial covariance matrix defined by (7) is used. To overcome this problem, the APES beamformer, which removes the desired signal from

the covariance matrix, has been introduced [22]. In APES beamforming, the weight $\mathbf{w}_{\text{APES}}$ is determined as follows:

$$\mathbf{w}_{\text{APES}} = \frac{\mathbf{Q}^{-1}\mathbf{a}}{\mathbf{a}^{\text{H}}\mathbf{Q}^{-1}\mathbf{a}}, \tag{10}$$

where $\mathbf{Q} = \mathbf{R} - \mathbf{G}\mathbf{G}^{\text{H}}$, and $\mathbf{G} = [g_0 \ g_1 \ g_2 \ ... \ g_{M-1}]^{\text{T}}$. The $\mathbf{G}$ corresponds to the desired signal, and in [22], all of the elements g_m ($m = 0, 1, ..., M - 1$) of vector $\mathbf{G}$ are estimated as $g_m = \mathbf{a}^{\text{H}}\mathbf{S}/M$.

C. Consideration of Element Directivity in Adaptive Beamforming

In the APES beamforming proposed in [22], the directivity of each transducer element is not considered (the transducer element is assumed to be omnidirectional). However, each element should have directivity owing to its finite size. Therefore, more components arising from the desired signal will remain in the covariance matrix $\mathbf{Q}$ when the accuracy in estimation of the desired signal is degraded due to the element directivity. Consequently, the desired signal in the output u_{APES} will be suppressed. In the present study, the directivity of each transducer element was considered to improve the accuracy in estimation of the desired signal $\mathbf{G}$ (i.e., the echo from the focal point) for a better removal of the desired signal from the covariance matrix.

As shown in Fig. 1, the direction from the mth transducer element to the focal point $(x_{\text{f}}, z_{\text{f}})$ is defined by θ_m. The directivity $D(\theta_m)$ of the mth transducer element ($m = 0, 1, 2, ..., M - 1$) is expressed as follows [23]:

$$D(\theta_m) = \frac{\sin\left(\frac{\pi l}{\lambda}\sin\theta_m\right)}{\frac{\pi l}{\lambda}\sin\theta_m}, \tag{11}$$

where

$$\theta_m = \tan^{-1}\left(\frac{x_{\text{f}} - x_m}{z_{\text{f}}}\right), \tag{12}$$

l is the width of each transducer element, and λ is the ultrasonic wavelength.

In the modified APES beamforming proposed in the present study, the vector $\mathbf{G} = [g_0 \ g_1 \ g_2 \ ... \ g_{m-1} \ g_m \ g_{m+1} \ ... \ g_{M-1}]^{\text{T}}$ corresponding to the estimate of the desired signal is obtained as follows:

$$g_m = \frac{D(\theta_m)\mathbf{a}^{\text{H}}\mathbf{S}}{\sum_{i=0}^{M-1} D(\theta_i)}. \tag{13}$$

On the basis of (10), the weight $\mathbf{w}_{\text{mAPES}}$ and the output u_{mAPES} of the modified amplitude and phase estimation beamformer are obtained using the vector $\mathbf{G}$ obtained by (13).
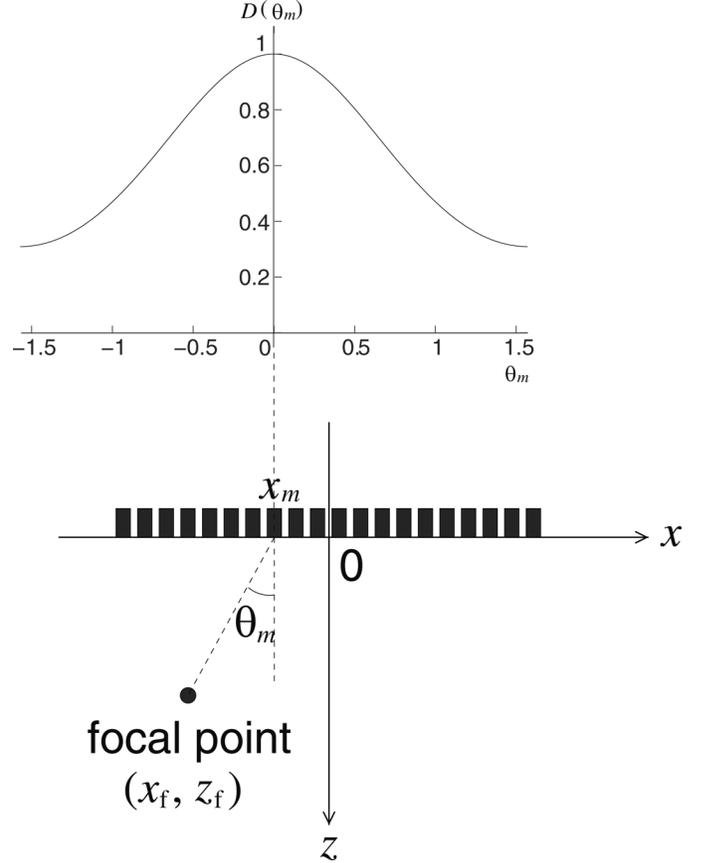

Fig. 1. Illustration of geometry. Directivity function $D(\theta_m)$ was calculated by (11) at $l = 150$ μm and $\lambda = 200$ μm.

$$\mathbf{w}_{\text{mAPES}} = \frac{\mathbf{Q}^{-1}\mathbf{a}}{\mathbf{a}^{\text{H}}\mathbf{Q}^{-1}\mathbf{a}}, \tag{14}$$

$$u_{\text{mAPES}} = \mathbf{w}_{\text{mAPES}}^{\text{H}}\mathbf{S}. \tag{15}$$

D. Sub-Aperture Beamforming for Reduction of Computational Load

In the present study, the modified APES beamformer along with sub-aperture beamforming was also examined for reduction of the computational load. The output y_k of the kth sub-aperture ($k = 0, 1, 2, ... K - 1$) consisting of $M_{\text{sub}} = M/K$ elements is expressed as follows:

$$y_k = \left(a_{M_{\text{sub}} \cdot k}^* \ a_{M_{\text{sub}} \cdot k+1}^* \ a_{M_{\text{sub}} \cdot k+2}^* \ \cdots \ a_{M_{\text{sub}} \cdot k+M_{\text{sub}}-1}^*\right)$$
$$\times \begin{pmatrix} s_{M_{\text{sub}} \cdot k} \\ s_{M_{\text{sub}} \cdot k+1} \\ s_{M_{\text{sub}} \cdot k+2} \\ \vdots \\ s_{M_{\text{sub}} \cdot k+M_{\text{sub}}-1} \end{pmatrix}$$
$$= \mathbf{a}_k^{\text{H}}\mathbf{S}_k. \tag{16}$$

In the present study, the output u_{mAPESsub} of the modified APES beamforming with sub-aperture beamforming was obtained as follows:

$$u_{\text{mAPESsub}} = \mathbf{w}_{\text{mAPESsub}} \mathbf{Y}, \tag{17}$$

where

$$\mathbf{Y} = \begin{pmatrix} y_0 & y_1 & \dots & y_{K-1} \end{pmatrix}^{\text{T}}, \tag{18}$$

$$\mathbf{w}_{\text{mAPESsub}} = \frac{\mathbf{C}^{-1}\mathbf{J}}{\mathbf{J}^{\text{H}}\mathbf{C}^{-1}\mathbf{J}}, \tag{19}$$

$$\mathbf{C} = \mathbf{Y}\mathbf{Y}^{\text{H}} - \mathbf{V}\mathbf{V}^{\text{H}}, \tag{20}$$

$$\mathbf{V} = \begin{pmatrix} v_0 & v_1 & \dots & v_{K-1} \end{pmatrix}^{\text{T}}, \tag{21}$$

$$v_k = \frac{b_k \sum_{i=0}^{K-1} y_i}{\sum_{i=0}^{K-1} b_i}, \tag{22}$$

$$b_k = \sum_{i=0}^{M_{\text{sub}}-1} D(\theta_{M_{\text{sub}} \cdot k + i}), \tag{23}$$

and $\mathbf{J}$ is a K dimensional vector of ones. Using sub-aperture beamforming, the dimensions of the covariance matrix $\mathbf{C}$ are reduced to $K \times K$. The difference between the procedures of the proposed method with and without sub-aperture beamforming is illustrated in Fig. 2.

E. Evaluation of Image Quality

In the present study, the quality of an obtained B-mode image was evaluated by methods described in [24], [25].

1) Spatial Resolution: The spatial resolution was defined as the lateral full-width at half-maximum of the amplitude profile of an echo from a point scatterer (point scatterer in simulation, fine wire in experiments).

2) Contrast: Contrast C was evaluated as follows:

$$C = \frac{|\mu_{\text{B}} - \mu_l|}{\frac{\mu_B + \mu_l}{2}}, \tag{24}$$

where u_{B} and μ_{l} are mean gray levels in background and lesion, respectively.

3) Contrast-to-Noise Ratio (CNR): Contrast-to-noise ratio was evaluated as follows:

$$\text{CNR} = \frac{|\mu_{\text{B}} - \mu_{\text{l}}|}{\sqrt{\frac{\sigma_{\text{B}}^2 + \sigma_{\text{l}}^2}{2}}}, \tag{25}$$

where σ_{B}^2 and σ_{l}^2 are variance of gray levels in background and lesion, respectively. Both in simulations and experiments, anechoic cyst phantoms were adopted as the lesion, and diffuse scattering medium was adopted as background.
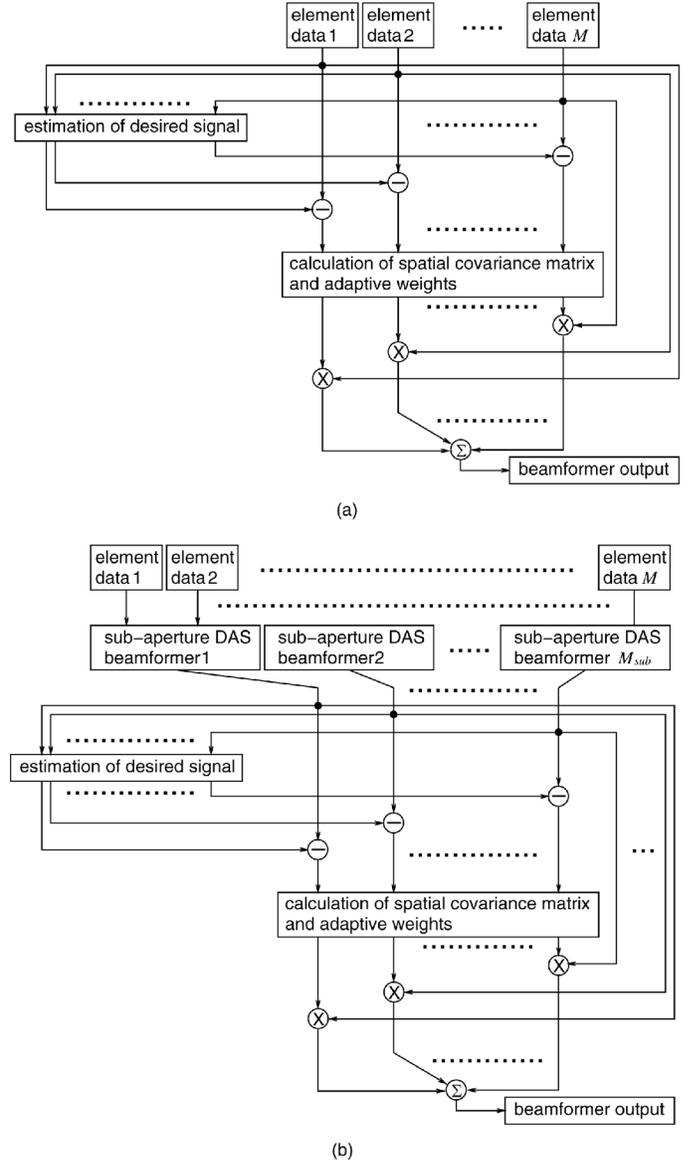

Fig. 2. Illustration of the proposed method with and without sub-aperture beamforming.

F. Method of Simulation

In the present study, the proposed method was evaluated by computer simulation and basic experiments using a phantom. In simulation, the scatterer distribution was generated by modifying the program, cyst_pht.m, provided by Field II [26]. The simulated phantom includes strong point scatterers and anechoic cysts. An in-house software was used for simulation of echoes from the generated scatterer distribution because Field II simulation does not incorporate with the element directivity. In the in-house software, the echo signal received by the jth transducer element $s_j(t)$ is obtained as follows:

$$s_j(t) = \sum_{i=1}^{M}\sum_{n=1}^{N} \frac{1}{r_i + r_j} A_n D(\theta_i) D(\theta_j) h(t - \tau_{\text{TBF},i} - \tau_i - \tau_j), \tag{26}$$
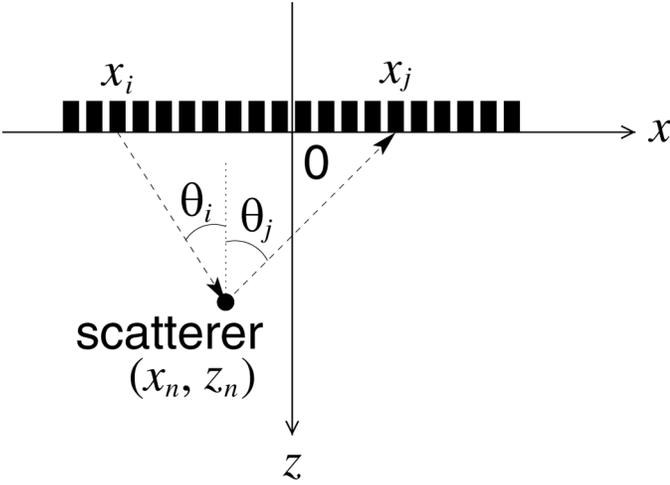
Fig. 3. Illustration of geometry in computer simulation.

where θ_i and θ_j are insonification and scattering angles illustrated in Fig. 3, M is the number of transmitting elements, N is the number of scatterers, and A_n is the scattering strength of the nth scatterer. The element directivity $D(\cdot)$ is obtained by (11). Each scatterer is located at (x_n, z_n) as illustrated in Fig. 3. Using the location of the transmitting and receiving elements $(x_i, 0)$ and $(x_j, 0)$, the distances r_i from the transmitting element to the scatterer and that r_j from the scatterer to the receiving element are expressed as follows:

$$r_i = \sqrt{(x_i - x_n)^2 + z_n^2}, \qquad (27)$$

$$r_j = \sqrt{(x_j - x_n)^2 + z_n^2}. \qquad (28)$$

In the present study, the time delay $\tau_{\text{TBF},i}$ applied to the ith transmitting element by the transmitting beamformer was set at zero because plane wave transmission was considered. The propagation delays τ_i and τ_j during transmission and reception are expressed as $\tau_i = r_i/c_0$ and $\tau_j = r_j/c_0$, respectively, where c_0 is speed of sound. The ultrasonic pulse $h(t)$ emitted from each transducer element is expressed as follows:

$$h(t) = \begin{cases} \left\{ 0.5 - 0.5\cos\left(\dfrac{2\pi t}{T_p}\right) \right\} \sin(2\pi f_0 t) & (0 \le t < T_{\text{p}}) \\ 0 & (\text{otherwise}), \end{cases} \qquad (29)$$

where f_0 is the center frequency of ultrasound set at 8 MHz, and T_{p} is the ultrasonic pulse duration corresponding to three cycles at ultrasonic center frequency. The element pitch and kerf were set at 0.2 and 0.05 mm, respectively. The signal-to-noise ratio of the simulated element RF signal was controlled by adding random noise.

G. Experimental Setup

An ultrasound imaging phantom (model 54GS, CIRS Inc., Norfolk, VA, USA) was used for evaluation of the

improvement of the imaging spatial resolution. A linear array ultrasonic probe at a nominal center frequency of 10 MHz (UST-5412, Aloka, Tokyo, Japan) was used, and ultrasonic echo signals received by individual transducer elements were acquired by a modified ultrasound scanner (α-10, Aloka) at a sampling frequency of 40 MHz. The beamforming procedure was performed off-line on the ultrasound echo signals received by the individual elements using an in-house software based on Matlab (The MathWorks Inc., Natick, MA, USA). The element pitch of the linear array was 0.2 mm, but the width l of each transducer element was not known. Therefore, the width l was assumed to be 0.15 mm.

The transmit-receive sequence is described in [3]. In the present study, the number of emissions of plane waves for creation of one image frame was set at 4, and each plane wave was emitted using 96 transducer elements. In each transmission, 24 focused receiving beams were created at intervals of 0.2 mm, and the aperture used to create one focused receiving beam consisted of $M = 72$ elements. Consequently, one image frame consisting of $24 \times 4 = 96$ focused receiving beams was obtained by four emissions of plane waves.

To obtain a complex element signal s_m of the mth element, in the present study, the discrete Fourier transform at $f_0 = 8.9$ MHz was applied to the real echo signal received by the mth element at every moment in time (corresponding to range distance) with a Hann window whose length was 0.225 μs. The computational cost of this procedure is similar to that of the quadrature demodulation and very effective to obtain the complex signal s_m.

In the present study, the time delay compensation defined by the steering vector **a** was performed by time shifting the obtained complex signal s_m. However, s_m is the discrete signal sampled at 40 MHz. Therefore, the residual sub-sample time delay $\Delta\tau_m$ was compensated by multiplying the time-shifted version of s_m by $\exp(2\pi f_0 \, \Delta\tau_m)$. After this time delay compensation, the steering vector **a** becomes a vector of ones.

III. Experimental Results

A. Simulation Experiments

Figs. 4(a), 4(b), and 4(c) show B-mode images of the phantom obtained by conventional DAS beamforming, APES beamforming, and modified APES beamforming proposed in the present study, respectively. The signal-to-noise ratio of the simulated RF signal was 40 dB. Fig. 5 shows lateral amplitude profiles at a range distance of 15 mm obtained by the respective methods. The lateral spatial resolutions evaluated from the lateral full widths at half maxima of the lateral amplitude profiles were 0.26 mm (DAS), 0.27 mm (APES), and 0.24 mm (modified APES). In conventional APES beamforming, the accuracy in estimation of the desired signal (the echo from the focal point) is degraded due to the lack of the information
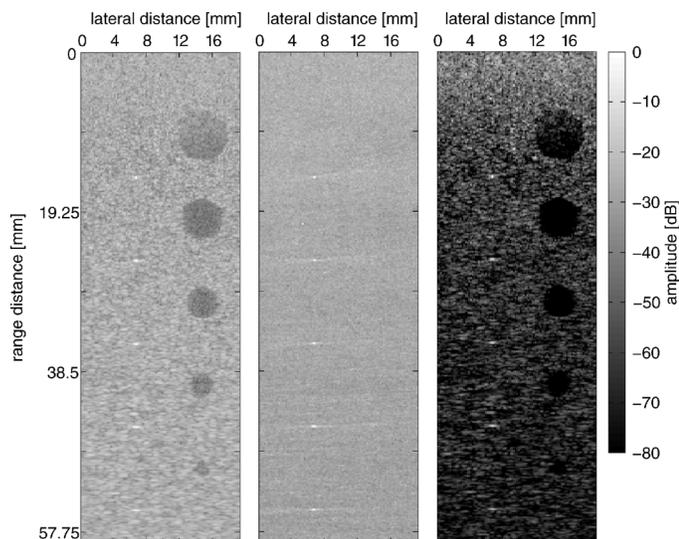
Fig. 4. B-mode images of simulated phantom obtained by (a) delay and sum beamforming (DAS), (b) amplitude and phase estimation beamforming (APES), and (c) modified amplitude and phase estimation beamforming (mAPES).
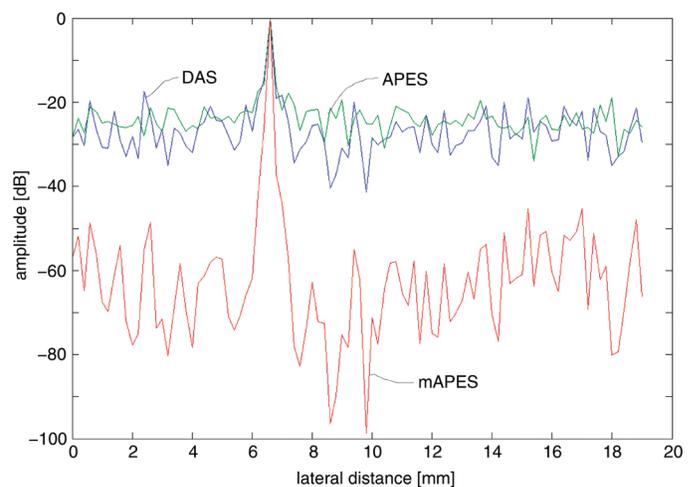

Fig. 5. Lateral amplitude profiles at a range distance of 15 mm in B-mode images shown in Fig. 4 obtained by delay and sum beamforming (DAS), amplitude and phase estimation beamforming (APES), and modified amplitude and phase estimation beamforming (mAPES).

on the element directivity, and the desired signals cannot be removed from the spatial covariance matrix $\mathbf{R}$. As a result, the desired signals are also suppressed by adaptive beamforming (particularly present with respect to strong echoes from wires). On the other hand, by considering the element directivity, more parts of the desired signals contained in the spatial covariance matrix $\mathbf{R}$ are removed, and as a result, the undesired signals are suppressed but the desired signals are not suppressed, as shown in Fig. 4(c).

In addition, C and CNR were estimated for evaluation of the image contrast. A rectangular region (from 19.3 to 21.2 mm in the range direction, from 14 to 16 mm in the lateral direction) was assigned as the lesion, and a rectangular region (from 19.3 to 21.2 mm in the range direction, from 8 to 10 mm in the lateral direction) was assigned as background (diffuse scattering medium). Obtained results (C, CNR) were (-8.5 dB, 6.6 dB; DAS), (-25.1 dB, -2.7 dB; APES), and (-6.1 dB, 2.1 dB; modified APES). In conventional APES beamforming, C and CNR are significantly degraded due to suppression of the desired signals. Using the proposed modified APES beamforming, C and

CNR are better than conventional APES beamforming but similar to DAS beamforming. In the modified APES beamforming, the spatial resolution was improved by suppressing the undesired signals. The suppression of the undesired signal also deepens dips between speckle echoes as shown in Fig. 4(c). The improvement in the spatial resolution yields a smaller speckle size, and the smaller speckle size reduces the mean gray level in diffuse scattering medium. Also, the deeper dips between speckle echoes increases the variance of gray levels. As a result, the C and CNR obtained by the modified APES beamforming did not outperform those obtained by DAS beamforming.

Table I shows lateral full widths at half maxima, C, and CNR obtained at different signal-to-noise ratios. Similar tendencies were observed at three different signal-to-noise ratios, but the conventional APES beamformer was more influenced by noise.

In the present study, the feasibility of sub-aperture beamforming was also examined. Fig. 6 shows B-mode images obtained by (top) APES beamforming and (bottom) modified APES beamforming, respectively, with (a) 24 sub-apertures, (b) 12 sub-apertures, and (c) 4 sub-apertures. Even with sub-aperture beamforming, the quality of the B-mode images could be significantly improved

TABLE I. Lateral Full Widths at Half Maxima (FWHM), Contrast, and Contrast-To-Noise Ratios (CNRs) Obtained at Different SNRs Using Delay and Sum (DAS), Amplitude and Phase Estimation (APES), and Modified Amplitude and Phase Estimation (mAPES) Beamforming.

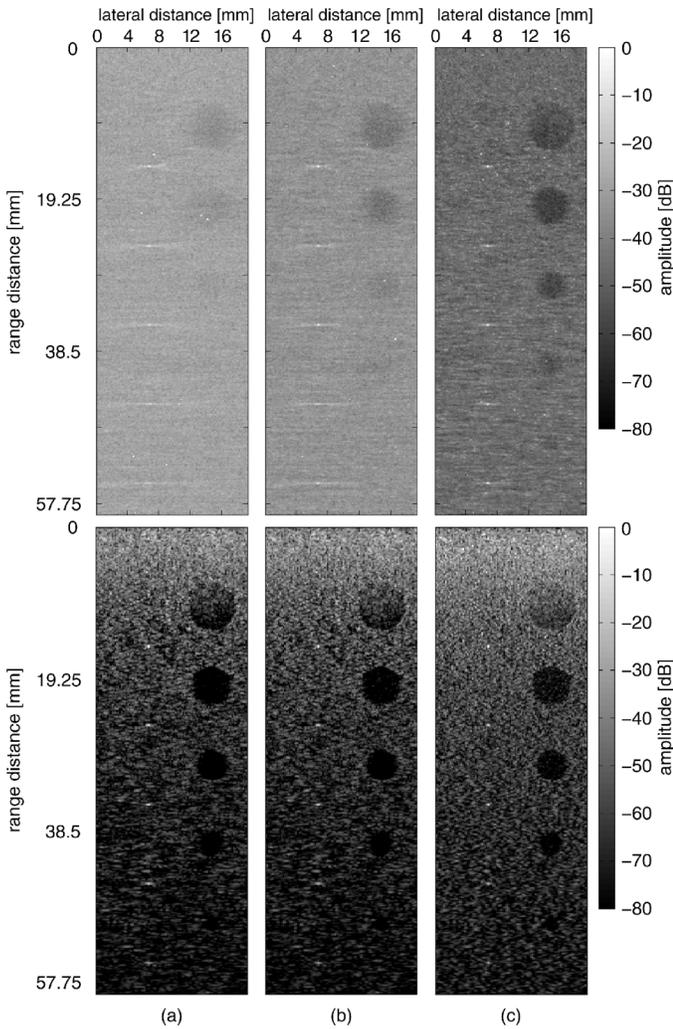| SNR [dB]	Beamformer	FWHM [mm]	Contrast [dB]	CNR [dB]
40	DAS	0.26	-8.5	6.6
	APES	0.27	-25.1	-2.7
	mAPES	0.24	-6.1	2.1
30	DAS	0.26	-8.6	6.6
	APES	0.28	-27.8	-5.9
	mAPES	0.24	-6.1	2.1
20	DAS	0.26	-8.7	6.5
	APES	0.27	-31.7	-9.4
	mAPES	0.24	-6.2	2.1

Fig. 6. B-mode images of simulated phantom obtained by (top) amplitude and phase estimation beamforming and (bottom) modified amplitude and phase estimation beamforming. (a) 24 sub-apertures, (b) 12 sub-apertures, (c) 4 sub-apertures.
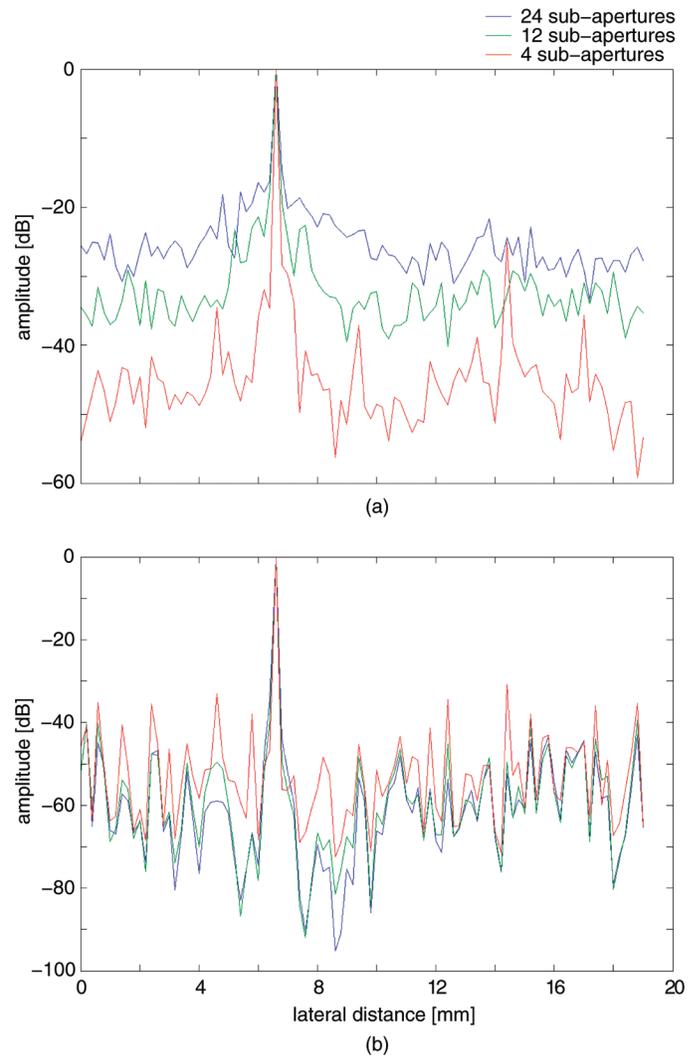

Fig. 7. Lateral amplitude profiles at a range distance of 15 mm in B-mode images shown in Fig. 6 obtained by (a) amplitude and phase estimation beamforming and (b) modified amplitude and phase estimation beamforming.

by considering the element directivity. Using sub-aperture beamforming, the dimensions of the covariance matrix are reduced, and the computational load can be significantly decreased. As can be seen in the lower image of Fig. 6(c), a good B-mode image can be obtained even with only 4 sub-apertures. Lateral amplitude profiles at a range distance of 15 mm obtained by APES beamforming and modified APES beamforming are shown in Figs. 7(a) and 7(b), respectively. In Fig. 7, the signal-to-noise ratio of the simulated RF signal was set at 40 dB.

Fig. 8 shows lateral full widths at half maxima (spatial resolution), contrast, and CNR at different numbers of sub-apertures and signal-to-noise ratios obtained by APES beamforming and modified APES beamforming. The evaluated performance metrics show that APES beamforming is more influenced by noise. The contrast obtained by modified APES beamforming is totally better than APES beamforming, but the CNRs obtained by APES beamforming with smaller numbers of sub-apertures were better than those obtained by modified APES

beamforming. In modified APES beamforming, the spatial resolution was not influenced by sub-aperture beamforming, but contrast and CNR were degraded slightly.

B. Basic Experiments

Figs. 9(a), 9(b), and 9(c) show B-mode images of the phantom obtained by conventional DAS beamforming, APES beamforming, and modified APES beamforming proposed in the present study, respectively. Fig. 10 shows lateral amplitude profiles at a range distance of 21 mm obtained by the respective methods. The lateral spatial resolutions evaluated from the widths at half maxima of the lateral amplitude profiles were 0.50 mm (DAS), 0.37 mm (APES), and 0.30 mm (modified amplitude and phase estimation). Similar tendency compared with the simulation experiment was obtained.

For evaluation of the image contrast, a phantom including an anechoic cyst was measured. Figs. 11(a), 11(b), and
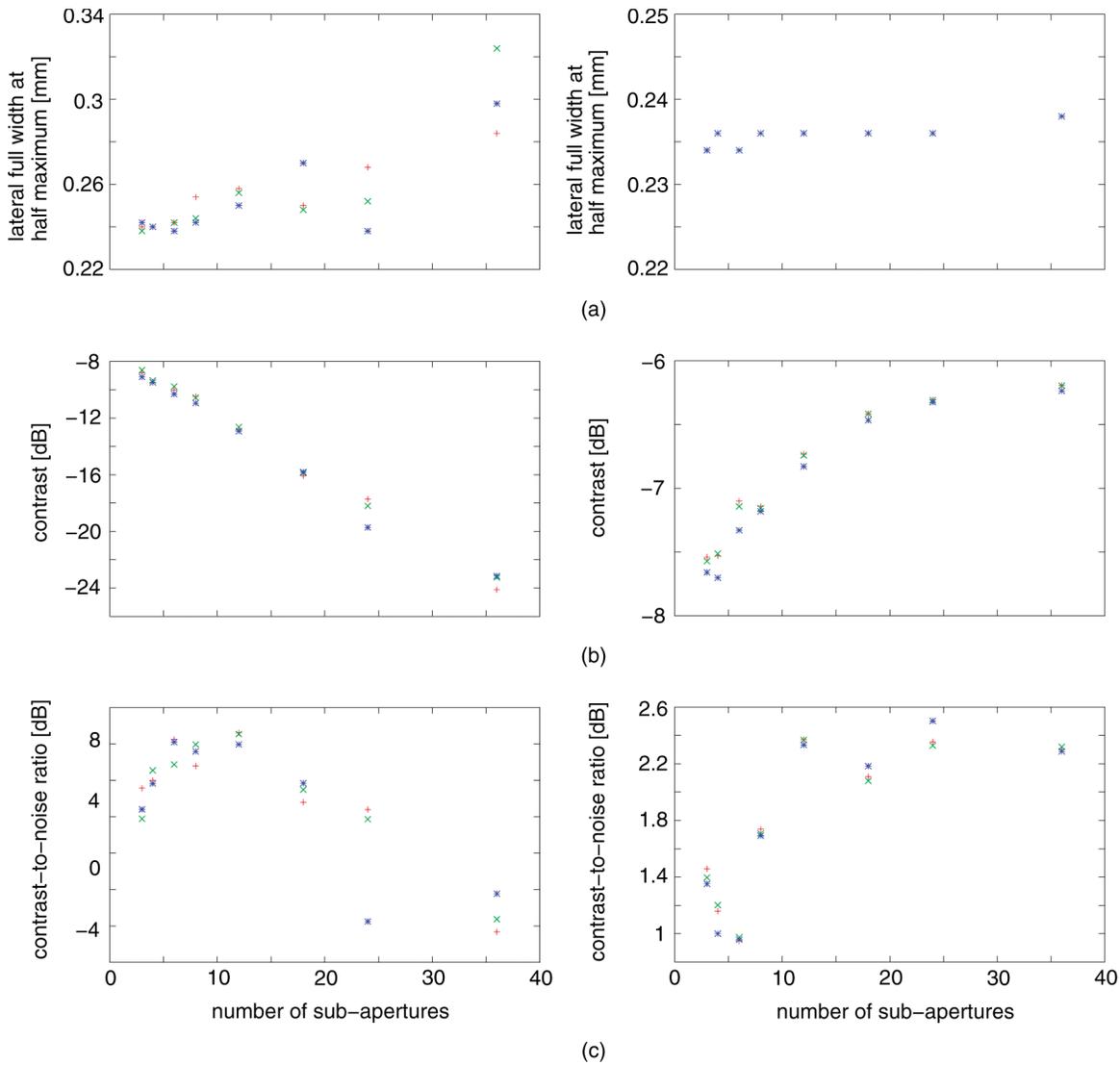
Fig. 8. Performance metrics obtained by (left) amplitude and phase estimation beamforming and (right) modified amplitude and phase estimation beamforming at different numbers of sub-apertures and signal-to-noise ratios (SNRs). (a) Lateral full widths at half maxima, (b) contrast, (c) contrast-to-noise ratios.

11(c) show B-mode images obtained by DAS beamforming, APES beamforming, and modified APES beamforming, respectively. A rectangular region (from 44.3 to 46.2 mm in the range direction, from 1 to 5 mm in the lateral direction) was assigned as the lesion, and a rectangular region (from 44.3 to 46.2 mm in the range direction, from 8 to 12 mm in the lateral direction) was assigned as background (diffuse scattering medium). Obtained results (C, CNR) were (−12.3 dB, 6.5 dB; DAS), (−32.8 dB, −11.3 dB; APES), and (−7.0 dB, 3.1 dB; modified APES). Results similar to those in simulation experiments were obtained.

The feasibility of sub-aperture beamforming was also examined. Fig. 12 shows B-mode images of the string phantom obtained by (top) APES beamforming and (bottom) modified APES beamforming, respectively, with (a) 24 sub-apertures, (b) 12 sub-apertures, and (c) 4 sub-apertures. Even with sub-aperture beamforming, the quality

of the B-mode images could be significantly improved by considering the element directivity. As can be seen in the lower image of Fig. 12(c), a good B-mode image can be obtained even with only 4 sub-apertures. Lateral amplitude profiles at a range distance of 21 mm obtained by APES beamforming and modified APES beamforming are shown in Figs. 13(a) and 13(b), respectively.

Fig. 14 shows B-mode images of the cyst phantom obtained by APES beamforming and modified APES beamforming, respectively, with (a) 24 sub-apertures, (b) 12 sub-apertures, and (c) 4 sub-apertures. A good B-mode image can be obtained even with only 4 sub-apertures.

Figs. 15(a), 15(b), and 15(c) show lateral full widths at half maxima, contrast, and CNRs obtained by APES beamforming and modified APES beamforming. The tendencies similar to those in the simulation experiments were observed. The evaluated performance metrics were improved by sub-aperture beamforming with a smaller
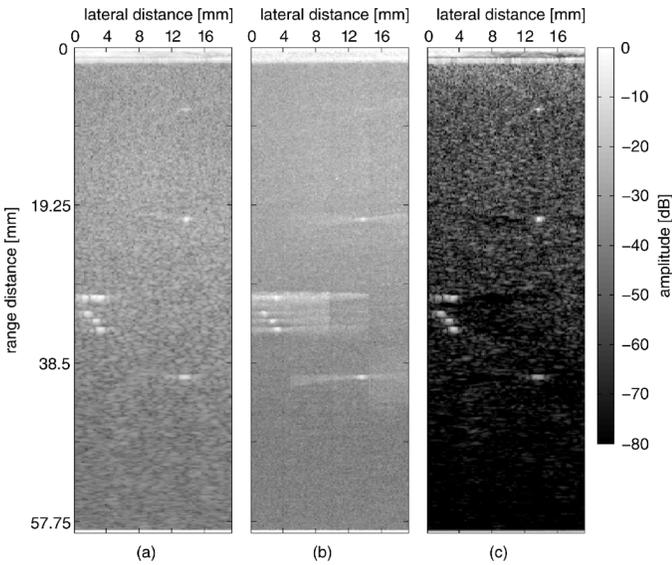
Fig. 9. B-mode images of string phantom obtained by (a) delay and sum beamforming (DAS), (b) amplitude and phase estimation beamforming (APES), and (c) modified amplitude and phase estimation beamforming (mAPES).

Fig. 11. B-mode images of cyst phantom obtained by (a) delay and sum beamforming (DAS), (b) amplitude and phase estimation beamforming (APES), and (c) modified amplitude and phase estimation beamforming (mAPES).

number of sub-aperture in APES beamforming. In modified APES beamforming, the performance metrics were much less influenced by the number of sub-apertures; the spatial resolution was slightly improved by a smaller number of sub-apertures. The contrast and contrast-to-noise ratio were slightly degraded by a smaller number of sub-apertures, as in the simulation experiments.

IV. Discussion

In minimum-variance-based adaptive beamforming, the components in the received signals, which correlate with the spatial covariance matrix, are suppressed. Therefore,
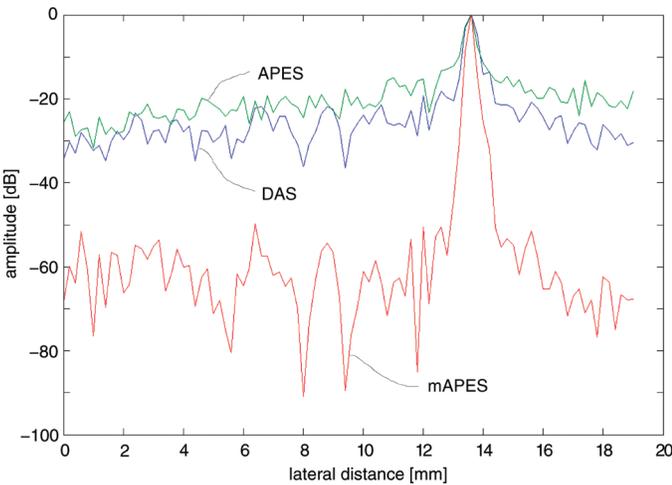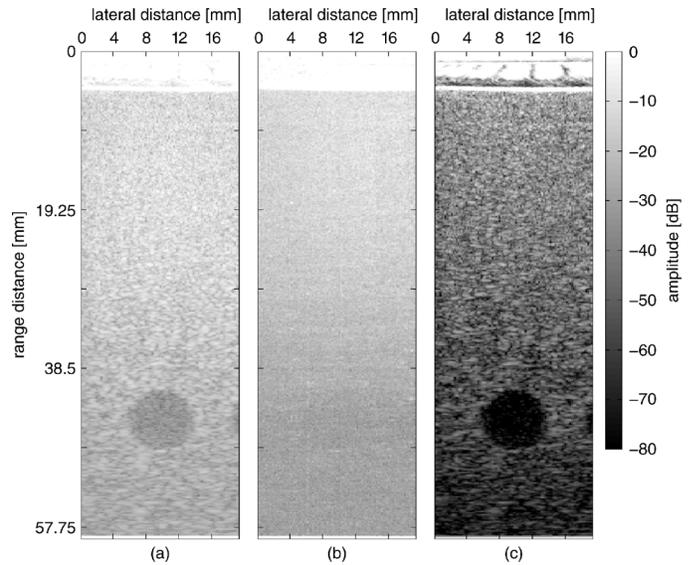

Fig. 10. Lateral amplitude profiles at a range distance of 21 mm obtained by delay and sum beamforming (DAS), amplitude and phase estimation beamforming (APES), and modified amplitude and phase estimation beamforming (mAPES).

only undesired signals should be contained in the spatial covariance matrix. However, the spatial covariance matrix is estimated by the measured signals, which contain the desired signal (echo from the focal point), and the desired signal would be suppressed by the adaptive beamforming process if no procedure for suppression of the desired signal contained in the spatial covariance matrix is used. In conventional minimum variance beamforming, the desired signal contained in the spatial covariance matrix is suppressed by sub-array averaging [14]. The APES beamformer proposes an alternative way for suppression of the desired signal contained in the spatial covariance matrix. The APES beamformer estimates the desired signal based on the concept of DAS beamforming and removes it from the spatial covariance matrix [22]. However, the conventional APES beamformer does not incorporate with the element directivity, and thus, the desired signal remains in the covariance matrix. In conventional APES beamforming described in [22], sub-array averaging was also used to further suppress the residual desired signal in the spatial covariance matrix. Using the conventional APES beamformer with sub-array averaging, B-mode images, which are significantly better than those obtained by DAS beamforming, can be obtained. Figs. 16(a) and 16(b) show B-mode images of the string and cyst phantoms obtained by conventional APES beamforming with sub-array averaging and diagonal loading. Each sub-array is composed of $L = 48$ elements (72 elements in the total aperture), and diagonal loading corresponding to $0.05/L$ of the received power [22] was used. As shown in Fig. 16, B-mode images obtained by conventional APES beamforming with sub-array averaging are much better than those obtained by DAS beamforming shown in Figs. 9 and 11.

In the present study, the accuracy in estimation of the desired signal contained in the spatial covariance matrix
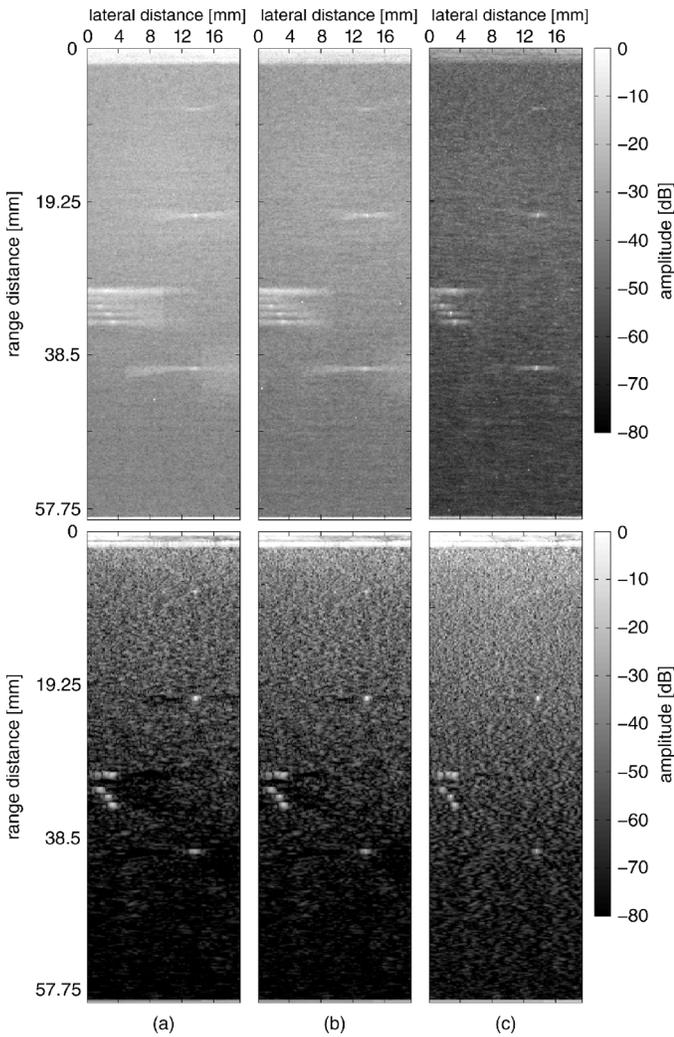
Fig. 12. B-mode images of string phantom obtained by (top) amplitude and phase estimation beamforming and (bottom) modified amplitude and phase estimation beamforming. (a) 24 sub-apertures, (b) 12 sub-apertures, (c) 4 sub-apertures.
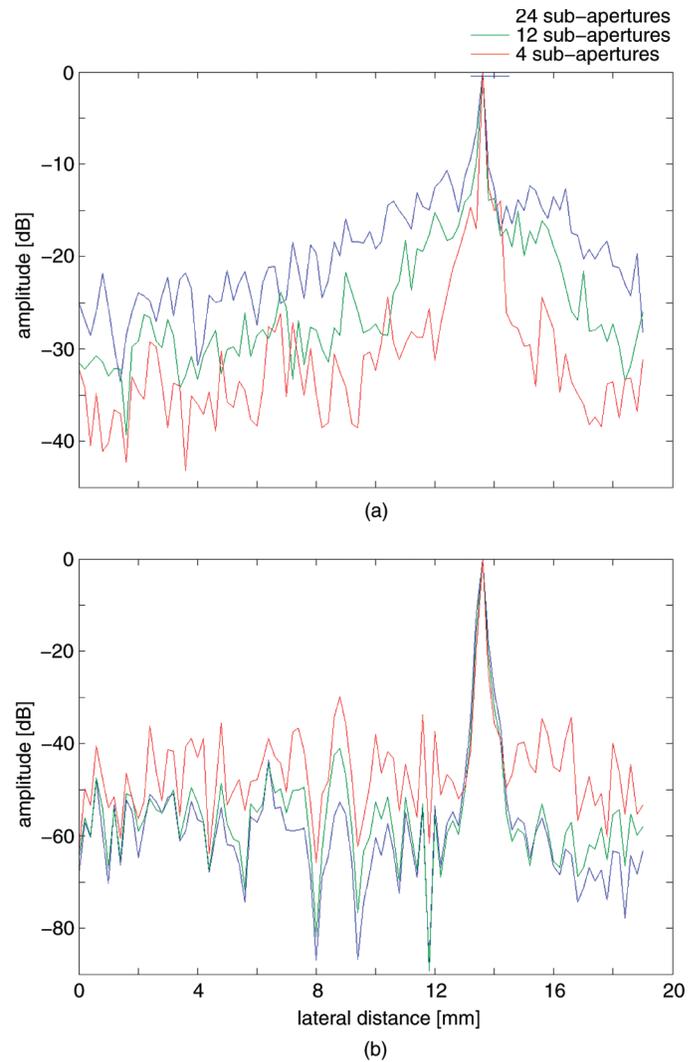
Fig. 13. Lateral amplitude profiles at a range distance of 21 mm obtained by (a) amplitude and phase estimation beamforming and (b) modified amplitude and phase estimation beamforming.

was improved by considering the element directivity. As a result, good B-mode images could be obtained without sub-array averaging, which was required for conventional APES beamforming [22]. The feasibility of the proposed method was examined through simulations and basic experiments. Sub-array averaging was not used for evaluation of the effect of the element directivity itself. In the proposed modified APES beamformer, in which the element directivity was taken into account, the spatial resolution and the image contrast were improved without sub-array averaging. In terms of the computational load, sub-aperture beamforming was used to increase the computational efficiency. The image spatial resolution is degraded when the computational load is reduced by sub-array averaging used in conventional adaptive beamforming (reduction of the size of the covariance matrix) [14]. In the present study, it was shown that sub-aperture beamforming did not degrade the spatial resolution and was computationally effective.

In the field of audible sound, the element directivity of a microphone array has been taken into account for determining the invariant (not adaptive) weights for individual elements in the beamforming process [27], [28]. In medical ultrasound imaging, the element directivity has not been considered in general. We have shown that the performance of the adaptive beamformer can be improved by considering the element directivity.

The adaptive beamformer suppresses the components contained in the covariance matrix, which is estimated from the received ultrasonic echo signals. Therefore, the desired signals should be removed from the covariance matrix. The accuracy in estimation of the desired signal is degraded if the element directivity is not considered. The amount of the desired signal component, which remains in the covariance matrix, is dominant when the desired signal is a strong echo, such as an echo from a wire in the experiment in the present study. In such a case, the dominant component contained in the covariance matrix
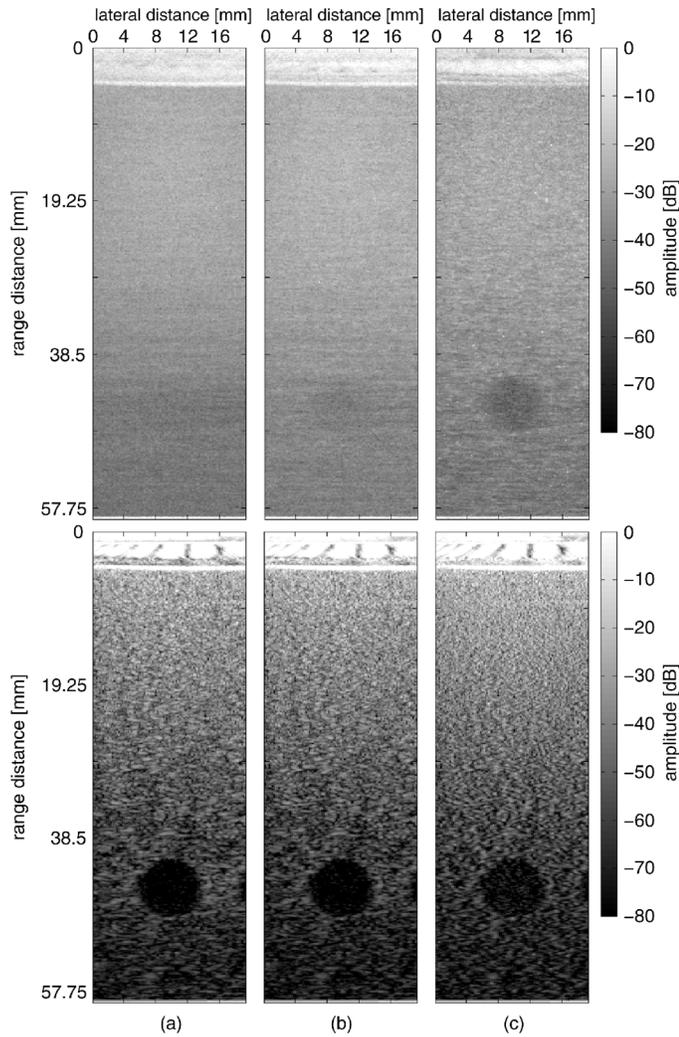
Fig. 14. B-mode images of cyst phantom obtained by (top) amplitude and phase estimation beamforming and (bottom) modified amplitude and phase estimation beamforming. (a) 24 sub-apertures, (b) 12 sub-apertures, (c) 4 sub-apertures.
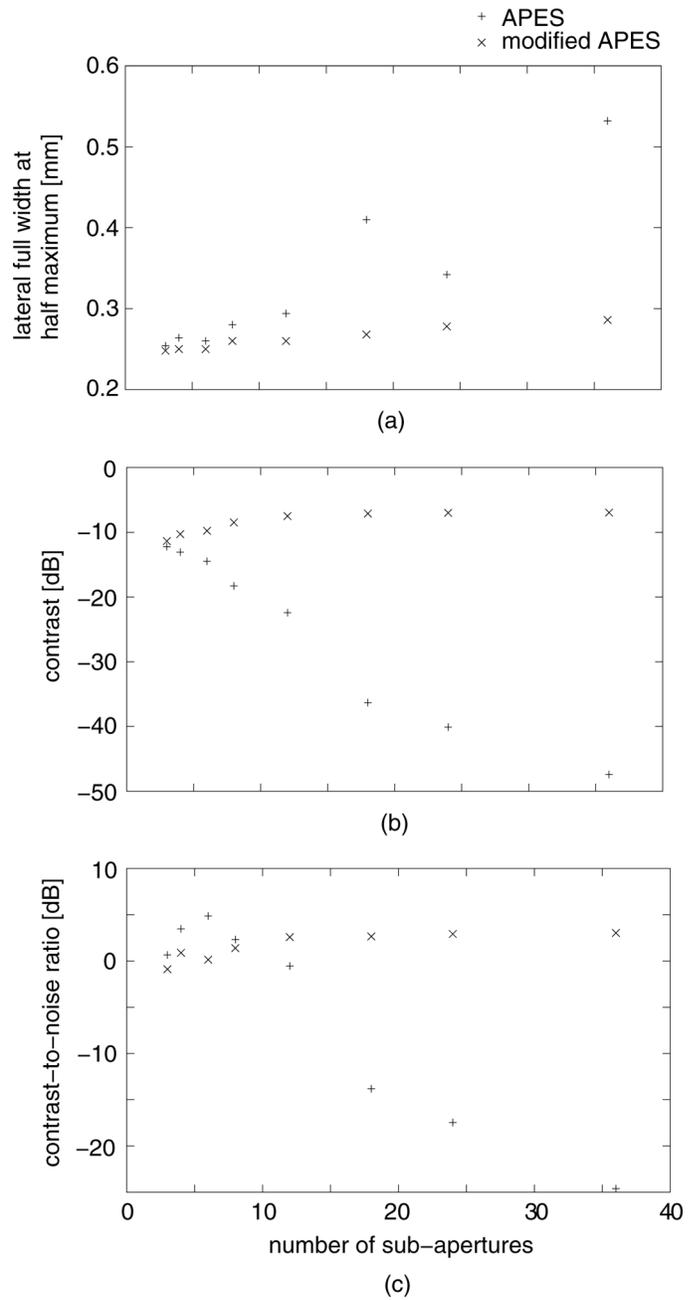

Fig. 15. Lateral full widths at half maxima (a), contrast (b), and contrast-to-noise ratios obtained by amplitude and phase estimation (APES) beamforming and modified APES with different numbers of sub-apertures.

becomes the residue of the desired signal. As a result, the strong echoes (desired signal) were particularly suppressed by adaptive beamforming when the element directivity was not considered.

In conventional APES beamforming, the estimation of the desired signal corresponds to DAS beamforming with rectangular apodization. Therefore, the side lobe components, which are undesired signals, are also estimated and removed from the covariance matrix. Therefore, the side lobe components are not suppressed so much in conventional APES beamforming.

By considering the element directivity, the accuracy in estimation of the desired signal (i.e., the echo from the focal point) is improved, and more parts of the desired signal are removed from the covariance matrix. On the other hand, the accuracy in estimation of the side lobe components is degraded by considering the element directivity because the directivity shown by (11) assumes the direction of the signal to be the direction of the focal point, whereas the side lobe components originate from the other

directions. As a result, the side lobe components remain in the covariance matrix and are suppressed by the modified APES beamformer proposed in the present study.

Conventional adaptive beamforming is often used with the sub-array averaging technique [15]. Sub-array averaging avoids the desired signals being suppressed and reduces the computational load but degrades the spatial resolution. In the modified APES beamformer, sub-aperture beamforming reduces the computational load but does not degrade the spatial resolution. Such characteristics of the modified APES beamformer are very practical to realize high temporal and spatial resolutions simultaneously. Un-
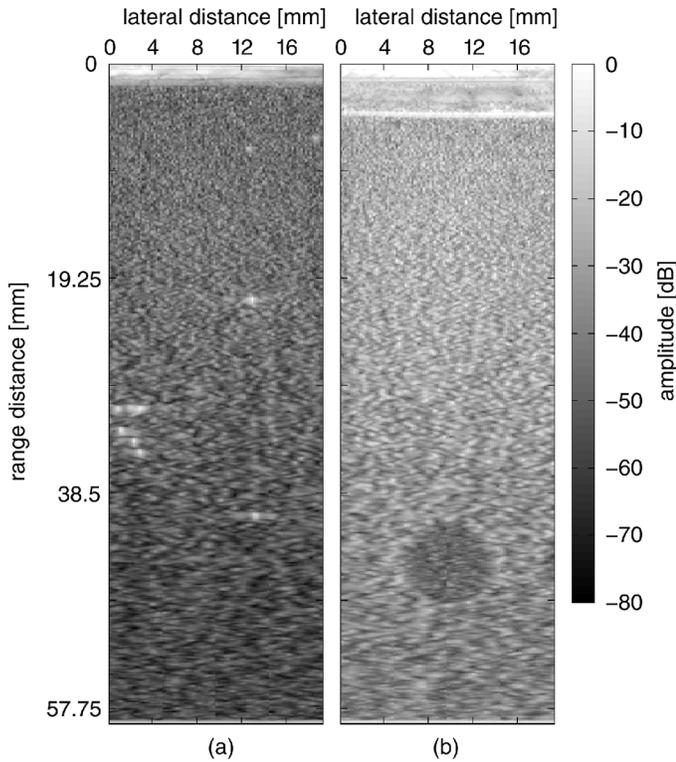
Fig. 16. B-mode images of (a) string and (b) cyst phantoms obtained by conventional APES beamforming with sub-array averaging (48 elements in each sub-array) and diagonal loading corresponding to $0.05/L$ of the received power.

estimated. Although ultrasonic attenuation during propagation was not considered, the spatial resolution and image contrast were improved significantly compared with conventional DAS and APES beamforming. Further study on incorporating with ultrasonic attenuation would realize more accurate estimation of the desired signal and additional improvement of the image quality.

In addition, sub-aperture beamforming was implemented for reduction of computational load. In minimum variance beamforming, sub-array averaging was used for reduction of computational load. However, sub-array averaging degraded the spatial resolution of an obtained ultrasound image. In contrast, sub-aperture beamforming used in the proposed modified APES beamformer did not degrade the spatial resolution. Also, as seen in Fig. 12, sub-aperture beamforming seems to improve the penetration depth. A larger number of elements in each sub-aperture realized a better penetration depth. The improvement of the signal-to-noise ratio of the output signal from each sub-aperture can be considered as a reason for the improvement in the penetration depth.

As described above, the proposed modified APES beamformer has preferable characteristics, i.e., providing better spatial resolution and contrast than conventional beamformer even with a 4×4 spatial covariance matrix. Further study should be conducted for real-time implementation of the proposed method. A GPU-based system is a potential candidate for real-time implementation [29].

der the computational environment in the present study, the computation time required for proposed beamforming with 4 sub-apertures (18 elements in each sub-aperture) was 1/20 of that required for proposed beamforming without sub-apertures (72 elements in total aperture). Calculation of the inverse matrix of the spatial covariance matrix of a large dimension is a significant computational load, and the sub-aperture beamforming is effective to reduce the dimension of the spatial covariance matrix.

One of the problems of the proposed modified APES beamformer is the excessive suppression of speckle echoes from diffuse scattering medium. As can be seen in Fig. 10, the difference between amplitudes of echoes from a strong scatterer (wire) and those of a diffuse scattering medium was significantly increased to about 60 dB. Although such a problem should be overcome in the future work, the proposed modified APES beamformer is effective for improvement of the spatial resolution in ultrasound imaging and is also computationally effective when working with sub-aperture beamforming.

V. Conclusions

In the present study, the APES beamformer was modified so that the accuracy in estimation of the desired signal is improved when the spatial covariance matrix was

References

[1] D. P. Shattuck, M. D. Weinshenker, S. W. Smith, and O. T. von Ramm, "Explososcan: A parallel processing technique for high speed ultrasound imaging with linear phased arrays," *J. Acoust. Soc. Am.*, vol. 75, no. 4, pp. 1273–1282, 1984.

[2] M. Tanter, J. Bercoff, L. Sandrin, and M. Fink, "Ultrafast compound imaging for 2-D motion vector estimation: Application to transient elastography," *IEEE Trans. Ultrason. Ferroelectr. Freq. Control*, vol. 49, no. 10, pp. 1363–1374, 2002.

[3] H. Hasegawa and H. Kanai, "Simultaneous imaging of artery-wall strain and blood flow by high frame rate acquisition of RF signals," *IEEE Trans. Ultrason. Ferroelectr. Freq. Control*, vol. 55, no. 12, pp. 2626–2639, 2008.

[4] Y. Honjo, H. Hasegawa, and H. Kanai, "Two-dimensional tracking of heart wall for detailed analysis of heart function at high temporal and spatial resolutions," *Jpn. J. Appl. Phys.*, vol. 49, no. 7, art. no. 07HF14, 2010.

[5] J. Provost, A. Gambhir, J. Vest, H. Garan, and E. E. Konofagou, "A clinical feasibility study of atrial and ventricular electromechanical wave imaging," *Heart Rhythm*, vol. 10, no. 6, pp. 856–862, 2013.

[6] D. Shahmirzadi, R. X. Li, and E. E. Konofagou, "Pulse-wave propagation in straight-geometry vessels for stiffness estimation: Theory, simulations, phantoms and *in vitro* findings," *J. Biomechan. Eng.*, vol. 134, no. 11, art. no. 114502, 2012.

[7] H. Hasegawa, K. Hongo, and H. Kanai, "Measurement of regional pulse wave velocity using very high frame rate ultrasound," *J. Med. Ultrasound*, vol. 40, no. 2, pp. 91–98, 2013.

[8] J. Bercoff, G. Montaldo, T. Loupas, D. Savery, F. Mézière, M. Fink, and M. Tanter, "Ultrafast compound Doppler imaging: Providing full blood flow characterization," *IEEE Trans. Ultrason. Ferroelectr. Freq. Control*, vol. 58, no. 1, pp. 134–147, 2011.

[9] B. Y. Yiu and A. C. Yu, "High-frame-rate ultrasound color-encoded speckle imaging of complex flow dynamics," *Ultrasound Med. Biol.*, vol. 39, no. 6, pp. 1015–1025, 2013.

[10] H. Takahashi, H. Hasegawa, and H. Kanai, "Echo speckle imaging of blood particles with high-frame-rate echocardiography," *Jpn. J. Appl. Phys.*, vol. 53, no. 7, art. no. 07KF08, 2014.

[11] S. K. Jespersen, J. E. Wilhjelm, and H. Sillesen, "Multi-angle compound imaging," *Ultrason. Imaging*, vol. 20, no. 2, pp. 81–102, 1998.

[12] G. Montaldo, M. Tanter, J. Bercoff, N. Benech, and M. Fink, "Coherent plane-wave compounding for very high frame rate ultrasonography and transient elastography," *IEEE Trans. Ultrason. Ferroelectr. Freq. Control*, vol. 56, no. 3, pp. 489–506, 2009.

[13] J. Capon, "High-resolution frequency-wavenumber spectrum analysis," *Proc. IEEE*, vol. 57, no. 8, pp. 1408–1418, 1969.

[14] J. F. Synnevåg, A. Austeng, and S. Holm, "Adaptive beamforming applied to medical ultrasound imaging," *IEEE Trans. Ultrason. Ferroelectr. Freq. Control*, vol. 54, no. 8, pp. 1606–1613, 2007.

[15] I. K. Holfort, F. Gran, and J. A. Jensen, "Broadband minimum variance beamforming for ultrasound imaging," *IEEE Trans. Ultrason. Ferroelectr. Freq. Control*, vol. 56, no. 2, pp. 314–325, 2009.

[16] J. F. Synnevåg, A. Austeng, and S. Holm, "Benefits of minimum-variance beamforming in medical ultrasound imaging," *IEEE Trans. Ultrason. Ferroelectr. Freq. Control*, vol. 56, no. 9, pp. 1868–1879, 2009.

[17] A. Rabinovich, Z. Friedman, and A. Feuer, "Multi-line acquisition with minimum variance beamforming in medical ultrasound imaging," *IEEE Trans. Ultrason. Ferroelectr. Freq. Control*, vol. 60, no. 12, pp. 2521–2531, 2013.

[18] J. F. Synnevåg, C.-I. Nilsen, and S. Holm, "Speckle statistics in adaptive beamforming," in *Proc. IEEE Ultrasonics Symp.*, 2007, pp. 1545–1548.

[19] J. F. Synnevåg, A. Austeng, and S. Holm, "A low-complexity data dependent beamformer," *IEEE Trans. Ultrason. Ferroelectr. Freq. Control*, vol. 58, no. 2, pp. 281–289, 2011.

[20] B. M. Asl and A. Mahloojifar, "A low-complexity adaptive beamformer for ultrasound imaging using structured covariance matrix," *IEEE Trans. Ultrason. Ferroelectr. Freq. Control*, vol. 59, no. 4, pp. 660–667, 2012.

[21] K. Kim, S. Park, J. Kim, S.-B. Park, and M. Bae, "A fast minimum variance beamforming method using principal component analysis," *IEEE Trans. Ultrason. Ferroelectr. Freq. Control*, vol. 61, no. 6, pp. 930–945, 2014.

[22] A. E. A. Blomberg, I. K. Holfort, A. Austeng, J. F. Synnevåg, S. Holm, and J. A. Jensen, "APES beamforming applied to medical ultrasound imaging," in *2009 IEEE Int. Ultrasonics Symp. Proc.*, pp. 2347–2350.

[23] F. J. Pompei and S. Wooh, "Phased array element shapes for suppressing grating lobes," *J. Acoust. Soc. Am.*, vol. 111, no. 5 pt. 1, pp. 2040–2048, 2002.

[24] M. C. van Wijk and J. M. Thijssen, "Performance testing of medical ultrasound equipment: Fundamental vs. harmonic mode," *Ultrasonics*, vol. 40, no. 1–8, pp. 585–591, 2002.

[25] J. M. Thijssen, G. Weijers, and C. L. de Korte, "Objective performance testing and quality assurance of medical ultrasound equipment," *Ultrasound Med. Biol.*, vol. 33, no. 3, pp. 460–471, 2007.

[26] J. A. Jensen, "Field: A program for simulating ultrasound systems," *Med. Biol. Eng. Comput.*, vol. 34, suppl. 1, pt. 1, pp. 351–354, 1996.

[27] M. R. P. Thomas, J. Ahrens, and I. Tashev, "Optimal 3D beamforming using measured microphone directivity patterns," in *International Workshop Acoust. Sig. Enhancement*, 2012.

[28] M. R. P. Thomas, J. Ahrens, and I. J. Tashev, "Beamformer design using measured microphone directivity patterns: Robustness to modeling error," in *APSIPA Ann. Summit Conf.*, 2012.

[29] J. P. Åsen, J. I. Buskenes, C.-I. C. Nilsen, A. Austeng, and S. Holm, "Implementing Capon beamforming on a GPU for real-time cardiac ultrasound imaging," *IEEE Trans. Ultrason. Ferroelectr. Freq. Control*, vol. 61, no. 1, pp. 76–85, 2014.

Hideyuki Hasegawa was born in Oyama, Japan, in 1973. He received the B.E. degree from Tohoku University, Sendai, Japan, in 1996. He received the Ph.D. degree from Tohoku University in 2001. He is presently an associate professor in Graduate School of Biomedical Engineering, Tohoku University. His research interest is medical ultrasonic imaging and measurements of tissue dynamics and viscoelasticity. Dr. Hasegawa is a member of the IEEE, the Acoustical Society of Japan, the Japan Society of Ultrasonics in Medicine, and the Institute of Electronics, Information and Communication Engineers.

Hiroshi Kanai was born in Matsumoto, Japan, on November 29, 1958. He received a B.E. degree from Tohoku University, Sendai, Japan, in 1981, and M.E. and the Ph. D. degrees, also from Tohoku University, in 1983 and in 1986, both in electrical engineering. From 1986 to 1988 he was with the Education Center for Information Processing, Tohoku University, as a research associate. From 1990 to 1992 he was a lecturer in the Department of Electrical Engineering, Faculty of Engineering, Tohoku University. From 1992 to 2001 he was an associate professor in the Department of Electrical Engineering, Faculty of Engineering, Tohoku University. Since 2001 he has been a professor in the Department of Electronic Engineering, Graduate School of Engineering, Tohoku University. Since 2008 he has been also a professor in the Department of Biomedical Engineering, Graduate School of Biomedical Engineering, Tohoku University. From 2012 he has been a dean of Graduate School of Engineering, Tohoku University.

His present interests are in transcutaneous measurement of the heart wall vibrations and myocardial response to propagation of electrical potential and cross-sectional imaging of elasticity around atherosclerotic plaque with transcutaneous ultrasound for tissue characterization of the arterial wall.

Dr. Kanai is a member of the Acoustical Society of Japan, a fellow of the Institute of Electronics Information and Communication Engineering of Japan, a member of the Japan Society of Ultrasonics in Medicine, Japan Society of Medical Electronics and Biological Engineering, and the Japanese Circulation Society. Since 1998, he has been a member of Technical Program Committee of the IEEE Ultrasonics Symposium. Since 2008, he has been an International Advisory Board of International Acoustical Imaging Symposium. Since 2011, he has been a Board member of International Congress on Ultrasonics. Since 2012, he has been an editor of *Journal of Medical Ultrasonics* and *Japanese Journal of Medical Ultrasonics*. Since 2013, he has been an associate editor of the *IEEE Transactions on Ultrasonics, Ferroelectrics, and Frequency Control*.